


Structure and α decay for the neutron-deficient nuclei with $89 \leq Z \leq 94$ in the density-dependent cluster model combined with a relativistic mean-field approach

Chen He and Jian-You Guo ^{*}*School of Physics and Optoelectronic Engineering, Anhui University, Hefei 230601, People's Republic of China* (Received 29 August 2022; revised 8 November 2022; accepted 1 December 2022; published 12 December 2022)

The density-dependent cluster model combined with relativistic mean-field theory is used to explore the structure and α decay for the neutron-deficient nuclei with $89 \leq Z \leq 94$, including two newly discovered nuclei ^{207}Th [*Phys. Rev. C* **105**, L051302 (2022)] and ^{214}U [*Phys. Rev. Lett.* **126**, 152502 (2021)]. The effective nucleon-nucleon interactions and matter density distributions from the relativistic mean field are employed to construct the α -daughter potential with a double-folding model. The Pauli blocking effect is considered by normalizing the strength of the α -daughter potential with the Bohr-Sommerfeld quantization condition. The α -preformation factor is calculated with the cluster formation model. The calculated α -decay half-lives for the 106 observed nuclei with $89 \leq Z \leq 94$ are in excellent agreement with experimental data. Extending this model to the unknown nuclei $^{201-204}\text{Ac}$, $^{205-206}\text{Th}$, $^{209-210}\text{Pa}$, $^{212-213,220}\text{U}$, $^{215-218,221}\text{Np}$, and $^{220-227}\text{Pu}$, the evolution of the $N = 126$ shell closure with neutron number is explored for the high- Z isotopes. The available α -decay energies, preformation factors, and α -decay half-lives show a regular change with increasing neutron number. Especially, the robustness of the $N = 126$ shell closure is shown up to the Pu isotopes.

DOI: [10.1103/PhysRevC.106.064310](https://doi.org/10.1103/PhysRevC.106.064310)

I. INTRODUCTION

The study of the structure and decay of neutron-deficient nuclei is one of the hottest frontier topics in nuclear physics. In the past decade, due to the development of radioactive beam facilities and the application of digital data acquisition systems worldwide, many new neutron-deficient nuclei were synthesized near the proton drip line. These newly synthesized neutron-deficient nuclei include ^{205}Ac [1], ^{207}Th [2], ^{211}Pa [3], $^{214-216,221}\text{U}$ [4–7], and $^{219,220,222-224}\text{Np}$ [8–12]. So far, experimentally, the proton-rich boundary $Z = 93$ has been reached. To explore the limit of neutron-deficient nuclei and investigate the robustness of the $N = 126$ shell closure away from the $Z = 82$ magic number, physicists have drawn the α -decay systematics for the isotopes near $N = 126$ with $89 \leq Z \leq 93$ [4,7,9], which support that the robustness of $N = 126$ shell closure up to the Np isotopes [8,10]. However, the systematics of the $N = 126$ shell closure has not been fully understood due to the absence of experimental data on the extremely proton-rich side, such as ^{220}U and ^{221}Np . The synthesis of new neutron-deficient heavy nuclei near $N = 126$ is challenging due to its extremely low yield and short lifetime. Therefore, it is necessary to investigate theoretically the evolution of $N = 126$ shell closure for the higher Z nuclei.

The study of α -decay can provide not only an effective means of identifying new neutron-deficient isotopes, but also an important way to obtain knowledge on nuclear structure [13,14]. With the accumulation of experimental data on α decay and the development of nuclear models, theoretical

studies of α decay are becoming more and more sophisticated. Since α decay is a quantum tunneling process [15,16], the interaction between the α particle and daughter nucleus plays a dominant role in this tunneling process. For this reason, many phenomenological and microscopic models have been developed to construct the α -daughter potential [17–21]. One of the most successful models is the double folding model [22], in which the α -daughter potential is constructed by folding the density distributions of the α particle and daughter nucleus with an effective nucleon-nucleon (NN) interaction. The essential part of this folding potential is the effective NN interaction, which is usually described by a phenomenological formula with parameters determined by fitting experimental data. Combining the α -daughter potential, Ren *et al.* have developed a density-dependent cluster model (DDCM) to describe α decay in a quasiclassical approximation. The available α -decay half-lives agree with the experimental data [23–25]. Recently, a Yukawa-type NN interaction from the relativistic-mean field (RMF) was successfully applied to the radioactive decay and fusion cross section of heavy ions [26–34]. Therefore, by using the Yukawa-type NN interaction from RMF instead of the phenomenological NN interaction in constructing the α -daughter potential, the DDCM should be more appropriate in describing α decay. For this reason, we develop the DDCM with the α -daughter potential constructed by the effective nucleon-nucleon interactions and matter density distributions from RMF.

In order to further improve the accuracy of DDCM calculations, the Pauli blocking effect needs to be considered. Considering that α clusters are mainly formed in the surfaces of nuclei, there is a significant density overlap between the α particle and daughter nucleus in the dense region, which is

^{*}jianyoun@ahu.edu.cn

caused by Pauli blocking [35]. The density overlap affects the inner region of the interaction potential between the α particle and daughter nucleus [36]. However, Pauli blocking is not embedded in the double-folding model, which fails in describing a process that is strongly influenced by the potential below the barrier in the internal region [37]. To compensate for the absence of Pauli blocking in the double-folding model, the Bohr-Sommerfeld quantization condition is used to normalize the strength of the effective NN interactions [38–40].

The α -preformation factor, which describes the formation probability of the α particle in the parent nucleus, plays an important role in α -decay lifetime. Accurate determination of preformation factor can help us to predict precisely α -decay half-lives [41–43], and obtain rich knowledge on nuclear structure [44,45]. For example, the shell closure around $Z = 82$ is clearly exposed in the α -preformation factor [44]. Since the formation of α particles involves nuclear many-body problems, it is difficult to calculate the preformation factor from microscopic models. Based on quantum mechanics theory, Ahmed *et al.* proposed a cluster formation model that can extract the preformation factor of even-even nuclei from the binding energy of the nucleus [46]. Ren *et al.* extended the model to the odd- A and odd-odd nuclei by introducing the contribution of unpaired nucleons, and confirmed the validity of the cluster formation model in the calculation of the α -preformation factor [44,47].

In the present work, we develop the DDCM for the description of α decay. The Yukawa-type NN interaction and matter density distributions from RMF are employed to construct the α -daughter potential with the double folding model. Combining the α -daughter potential from RMF into DDCM, the developed DDCM is used to investigate the α decay for the neutron-deficient nuclei with $89 \leq Z \leq 94$. To confirm the applicability of the present model, the DDCM based on a widely used M3Y-Paris effective NN interaction and the universal decay law (UDL) formula are also used to investigate the α decay for comparison. For the calculations in this paper, the experimental half-lives and Q_α values are mainly taken from the latest NUBASE2020 and AME2020 [48–50] compilations. The binding energies and Q_α values of unknown nuclei are obtained from the Weizsäcker-Skyrme-4 (WS4) model with radial basis function (RBF) correction [51], which is the model with the highest accuracy in describing nuclear mass. The α -preformation factor is calculated with the cluster formation model.

This article is organized as follows: Section II presents the theoretical framework of DDCM in combination with the relativistic mean field and the cluster formation model. The numerical results and discussions are given in Section III. A summary is given in Section IV.

II. THEORETICAL FRAMEWORK

α decay is related to the tunneling probability of an α particle and the α -preformation factor. Here, the DDCM in combination with RMF is used to calculate the tunneling probability of an α particle, and the cluster formation model is adopted to compute the α -particle preformation factor. For

simplicity in the following discussions, we sketch the theoretical framework of the two models.

A. The density-dependent cluster model in combination with the relativistic mean field

In the DDCM, the effective α -daughter potential consists of nuclear $V_N(R)$, Coulomb $V_C(R)$, and the centrifugal potentials,

$$V_T(R) = \lambda V_N(R) + V_C(R) + \frac{\hbar^2}{2\mu} \frac{(\ell + \frac{1}{2})^2}{R^2}, \quad (1)$$

where R is the distance of mass center between the α particle and the daughter nucleus, and μ is the reduced mass of the α particle in the α -daughter system. The last term is the Langer modified centrifugal barrier [52]. ℓ is the angular momentum taken away by the α particle.

The α -particle emission from parent nuclei obeys the spin-parity selection rules [53]

$$\ell = \begin{cases} \Delta_j & \text{for even } \Delta_j \text{ and } \pi_p = \pi_d, \\ \Delta_j + 1 & \text{for even } \Delta_j \text{ and } \pi_p \neq \pi_d, \\ \Delta_j & \text{for odd } \Delta_j \text{ and } \pi_p \neq \pi_d, \\ \Delta_j + 1 & \text{for odd } \Delta_j \text{ and } \pi_p = \pi_d, \end{cases} \quad (2)$$

where $\Delta_j = |j_p - j_d|$. j_p and π_p are the spin and parity of parent nucleus. j_d and π_d are the spin and parity of daughter nuclei.

The nuclear potential $V_N(R)$ is obtained with the double-folding model by folding the density distributions of the α particle and daughter nuclei with an effective NN interaction [22],

$$V_N(R) = \lambda \iint \rho_\alpha(\vec{r}_\alpha) v_{\text{NN}}(s) \rho_d(\vec{r}_d) d\vec{r}_\alpha d\vec{r}_d, \quad (3)$$

where $s = |\vec{R} + \vec{r}_\alpha - \vec{r}_d|$ corresponds to the distance between two specified interaction points of α particle and daughter nucleus. ρ_α and ρ_d are the density distributions of α particle and daughter nuclei, respectively. Considering that the RMF theory is very successful in describing the ground properties of nuclei [54–56], here we calculate the densities of α particle and daughter nuclei with the RMF theory. The reliability of RMF in calculating density has been tested in the construction of nuclear potentials with the double-folding model [34,57,58].

The effective NN interaction $v_{\text{NN}}(s)$ is obtained from the RMF calculations. The details can be seen in Refs. [26–33]. The expression of the NN interaction is presented as

$$v_{\text{NN}}^{\text{RMF}}(s) = \frac{g_\omega^2}{4\pi} \frac{\exp(-m_\omega s)}{s} + \frac{g_\rho^2}{4\pi} \frac{\exp(-m_\rho s)}{s} - \frac{g_\sigma^2}{4\pi} \frac{\exp(-m_\sigma s)}{s} + \frac{g_2^2}{4\pi} s \exp(-2m_\sigma s) + \frac{g_3^2}{4\pi} \frac{\exp(-3m_\sigma s)}{s} - J_{00} \delta(\vec{s}), \quad (4)$$

where m_ω , m_ρ , and m_σ are the masses of ω , ρ , and σ mesons multiplied by sc/\hbar . g_ω , g_ρ , and g_σ are the interaction strengths of the corresponding mesons. g_2 and g_3 are the nonlinear self-coupling coefficients of the σ meson.

For comparison, the widely used M3Y-Paris effective NN interaction [22] is introduced as

$$v_{\text{NN}}^{\text{M3Y}}(s) = 11061.625 \frac{\exp(-4s)}{4s} - 2537.5 \frac{\exp(-2.5s)}{2.5s} - J_{00} \delta(\vec{s}), \quad (5)$$

where $J_{00} = 592 \text{ MeV fm}^3$ [59].

To compensate for the Pauli blocking effect, the normalizing factor λ is introduced, and is determined by the Bohr-Sommerfeld quantization condition [38–40]

$$\int_{R_1}^{R_2} \sqrt{\frac{2\mu}{\hbar^2} |V_T(R) - Q_\alpha|} dR = (2n+1) \frac{\pi}{2} = (G-l+1) \frac{\pi}{2}, \quad (6)$$

where Q_α is the α -decay energy, R_i ($i = 1, 2, 3$) are classical turning points for the α -daughter-nucleus potential barrier, obtained by $V_T(R)_{R=R_i} = Q_\alpha$. The global quantum number G is determined by the Wildermuth condition [60]:

$$G = 2n + l = \sum_{i=1}^4 g_i, \quad (7)$$

where g_i is the oscillator quantum number of the α particle, and n is the node number of the α -core wave function. For the α decay, there are $G = 22(N > 126)$, $G = 20(82 < N \leq 126)$, and $G = 18(N \leq 82)$, which can be found in Ref. [61].

The Coulomb potential $V_C(R)$ is obtained by double folding model with the proton-proton Coulomb interaction $v_C(s)$ and the charge densities ($\rho_{p\alpha}$, ρ_{pd}) as

$$V_C(R) = \iint \rho_{p\alpha}(\vec{r}_\alpha) v_C(s) \rho_{pd}(\vec{r}_d) d\vec{r}_\alpha d\vec{r}_d. \quad (8)$$

After determining the normalizing factor λ , the total α -daughter potential is obtained. The Wentzel-Kramers-Brillouin (WKB) approximation is employed to calculate the tunneling probability of the α particle:

$$P = \exp\left(-2 \int_{R_2}^{R_3} dR \sqrt{\frac{2\mu}{\hbar^2} |V_T(R) - Q_\alpha|}\right). \quad (9)$$

The assault frequency ν can be written as the inverse of the time required to traverse the distance back and forth between the turning points R_1 and R_2 as [62]

$$\nu = T^{-1} = \frac{\hbar}{2\mu} \left[\int_{R_1}^{R_2} \frac{dR}{\sqrt{\frac{2\mu}{\hbar^2} (|V_T(R) - Q_\alpha|)}} \right]^{-1}. \quad (10)$$

The α -decay width can be calculated with $\Gamma = \hbar P \nu P_\alpha$, where P_α is the preformation probability of an α particle in a parent nucleus, which is derived from the cluster formation model. Finally, the α -decay half-lives are obtained with $T_{1/2} = \hbar \ln 2 / \Gamma$.

To check the superiority of the present model, we also calculate the α -decay half-lives with an empirical UDL formula [63,64]:

$$\log_{10} T_{1/2}(s) = a Z_\alpha Z_d \sqrt{\frac{A_\alpha A_d}{(A_\alpha + A_d) Q_\alpha}} + b \sqrt{\frac{A_\alpha A_d}{(A_\alpha + A_d)} Z_\alpha Z_d (A_\alpha^{1/3} + A_d^{1/3})} + c, \quad (11)$$

where the parameters a , b , and c are determined by fitting experimental data [63,64].

B. Cluster formation model

In the cluster formation model [46,47], the initial state Ψ of parent nuclei can be defined as a linear superposition of N possible clusterization states Ψ_i . The Hamiltonian H_i for each clusterization configuration constitutes the total Hamiltonian H ,

$$\Psi = \sum_{i=1}^N a_i \Psi_i, \quad H = \sum_{i=1}^N H_i, \quad (12)$$

where a_i is the superposition coefficient. Since each clusterization state describes the same nucleus, all these states should share the same eigenenergy, which is equal to the eigenenergy E . Considering the orthonormality of these clusterization states, there is the relationship between the eigenenergy E and the superposition coefficient a_i :

$$E = \sum_i |a_i|^2 E = \sum_i E_i^f, \quad (13)$$

where E_i^f is the formation energy of the cluster in the clusterization state Ψ_i . Thus, the probability of α clusterization, P_α , can be expressed as

$$P_\alpha = |a_\alpha|^2 = \frac{E_\alpha^f}{E}, \quad (14)$$

where E_α^f denotes the formation energy of the α cluster. The total energy E is composed of E_α^f and the interaction energy between the α cluster and residual nucleons. Both the formation energy E_α^f and the total energy E are calculated by solving the corresponding Schrödinger equation. By analyzing the surface nucleon-nucleon interactions, Deng *et al.* proposed a comprehensive formula to extract the formation energy for even-even, odd-A, and odd-odd nuclei [44,47]:

$$E_\alpha^f = \begin{cases} 2S_p + 2S_n - S_\alpha & (\text{even-even}), \\ 2S_p + S_{2n} - S_\alpha & (\text{even-odd}), \\ S_{2p} + 2S_n - S_\alpha & (\text{odd-even}), \\ S_{2p} + S_{2n} - S_\alpha & (\text{odd-odd}), \end{cases} \quad (15)$$

where S_p (S_n), S_{2p} (S_{2n}), and S_α are the one-proton (neutron) separation energy, the two-proton (neutron) separation energy,

and α cluster separation energy, defined as

$$\begin{aligned} S_p(A, Z) &= B(A, Z) - B(A - 1, Z - 1), \\ S_n(A, Z) &= B(A, Z) - B(A - 1, Z), \\ S_{2p}(A, Z) &= B(A, Z) - B(A - 2, Z - 2), \\ S_{2n}(A, Z) &= B(A, Z) - B(A - 2, Z), \\ S_\alpha(A, Z) &= B(A, Z) - B(A - 4, Z - 2), \end{aligned} \quad (16)$$

where $B(A, Z)$ is the binding energy of a nucleus with mass number A and proton number Z . The binding energies of known nuclei are taken from the recently updated atomic mass evaluation tables AME2020 [49,50]. For those unknown nuclei, the binding energies are obtained by the WS4+RBF mass model [51].

III. DISCUSSION

Based on the previous formalism, we calculate the α -decay half-lives for the neutron-deficient nuclei with $89 \leq Z \leq 94$. Since the α -decay half-lives are related to the probability of the α particle penetrating the potential barrier and the preformation factor of the α particle in a parent nucleus, it is necessary to obtain the α -daughter potential and α -particle preformation factor. Here, we first introduce the construction of the α -daughter potential. Based on the nucleon-nucleon interactions and matter density distributions from RMF, the double-folding model is used to construct the α -daughter potential. To compensate for the absence of the Pauli blocking effect, the Bohr-Sommerfeld quantization condition is used to normalize the strength of the nuclear potential. The α -particle preformation factor is calculated with the cluster formation model, which has been widely used to extract the α -particle preformation factor for the even-even, odd- A , and odd-odd nuclei. For convenience in the following discussions, the nuclear potential based on the matter density distributions and the effective NN interaction from the RMF calculations is called V_N^{RMF} . The corresponding effective α -daughter potential is labeled as V_T^{RMF} . For comparison, the M3Y-Paris effective NN interactions are also used to construct the nuclear potential and α -daughter potential with the double-folding model. The nuclear potential based on the matter density distributions from the RMF calculations and the effective M3Y-Paris NN interactions is called V_N^{M3Y} , and the effective α -daughter potential is labeled V_T^{M3Y} .

In order to confirm that the α -daughter potential constructed by the present method is appropriate to describe α decay, we plot the nuclear potential and α -daughter potential in Fig. 1 for the latest synthesized neutron-deficient nucleus ^{207}Th as an illustrative examples. In calculating the α -daughter potential, the Bohr-Sommerfeld quantization condition in Eq. (6) is used; the calculated intensity parameters are $\lambda^{\text{RMF}} = 0.593$ and $\lambda^{\text{M3Y}} = 0.548$. From Fig. 1, it can be seen that V_N^{RMF} is similar to V_N^{M3Y} . Since M3Y-Paris is a widely used effective NN interaction, with the matter density distributions from the RMF calculations, the nuclear potential V_N^{M3Y} should be fairly realistic. Hence, the similarity of these two potentials suggests that both of them are favorable nuclear potentials. Nevertheless, there

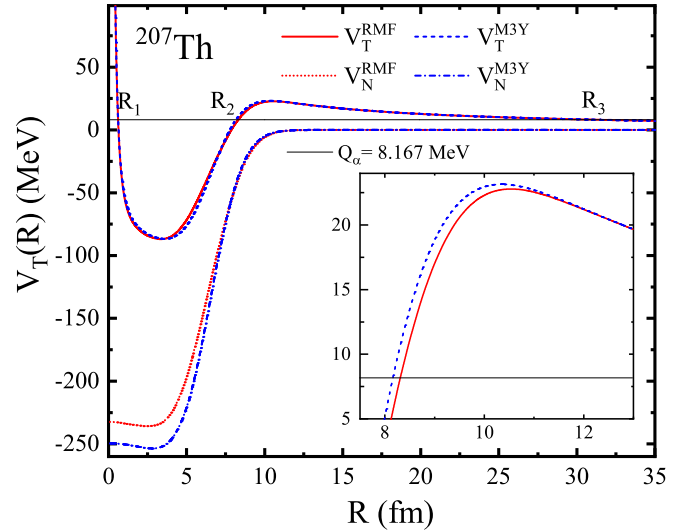


FIG. 1. The constructed nuclear potential and α -daughter potential with the double-folding model for the latest synthesized neutron-deficient nucleus ^{207}Th as an illustrative example. V_N^{RMF} and V_T^{RMF} denote the nuclear potential and α -daughter potential with the matter density distributions and the effective NN interactions from the RMF calculations. V_N^{M3Y} and V_T^{M3Y} present the nuclear potential and α -daughter potential with the RMF matter density distributions and the effective M3Y-Paris NN interactions. The inset shows the classical turning point and barrier height.

are some differences between the nuclear potential V_N^{RMF} from the RMF NN interactions and those V_N^{M3Y} from the M3Y NN interactions. In the interval from R_1 to the complete overlap (about 12 fm), V_N^{RMF} is a little different from V_N^{M3Y} . Since the Coulomb potential and centrifugal

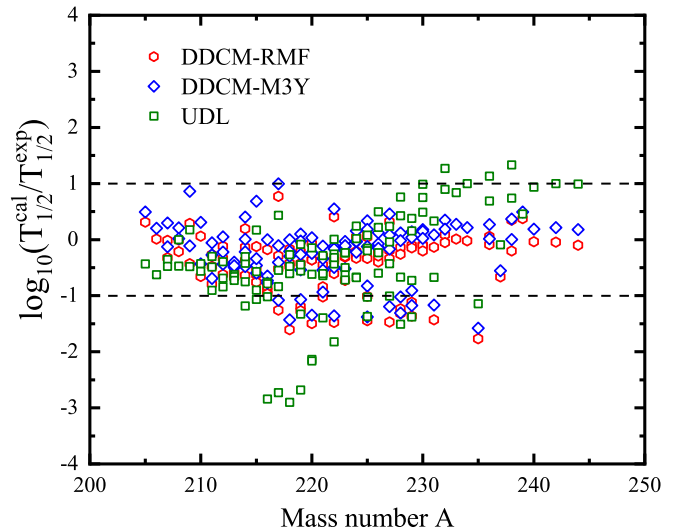


FIG. 2. The logarithms of the ratio of calculated α -decay half-lives to experimental data for the 106 known Ac, Th, Pa, U, Np, and Pu isotopes. The results from the DDCM-RMF calculations, the DDCM-M3Y calculations, and the empirical UDL formula are shown as red hexagons, blue rhombuses, and green squares, respectively.

potential are independent of the NN interactions, the differences in the nuclear potentials lead to the differences in the α -daughter potentials. The significant differences appear in the height and position of α -daughter potentials. The height and position in V_T^{RMF} are 22.789 MeV and $R = 10.49$ fm, while those in V_T^{M3Y} are 23.153 MeV and $R = 10.39$ fm. Compared with V_T^{M3Y} , in addition to the lower barrier height, the barrier V_T^{RMF} is narrower, which tends to favor barrier penetration. Based on V_T^{RMF} , with the DDCM used to calculate the α -decay half-lives, the α -decay half-life for ^{207}Th is 9.43 ms. Similarly, based on V_T^{M3Y} , the calculated α -decay half-life is 19.24 ms. Compared with the experimental datum 9.70 ms, the α -daughter potential from the RMF NN interactions is superior to that from the M3Y NN interactions.

To confirm that V_T^{RMF} is an effective α -daughter potential, we combine it with DDCM to calculate the α -decay half-lives for the 106 known Ac, Th, Pa, U, Np, and Pu isotopes. For convenience, the α -decay half-lives calculated with DDCM based on V_T^{RMF} are called DDCM-RMF calculations, and those based on V_T^{M3Y} are referred to as DDCM-M3Y calculations. The calculated α -decay half-lives are listed in Table I. The first column represents the specified α decay. The second column denotes the spins and parities of the parent and daughter nuclei, which are extracted from Refs. [48,65]. The third column is the angular momentum calculated using Eq. (2). The α -decay energies and the α -preformation factors are given in the fourth and fifth columns, respectively. The experimental α -decay half-lives are listed in the sixth column. The α -decay half-lives in the DDCM-RMF calculations, the DDCM-M3Y calculations, and the empirical UDL formula are listed in the seventh, eighth, and ninth columns, respectively. In the calculation with UDL, the adopted parameters are the same as in Refs. [63,64]. From Table I, it can be seen that the calculated α -decay half-lives in the three models are considerably consistent with the experiment data. The deviations of theoretical calculations and experiments are much less than an order of magnitude with a few exceptions. Detailed observations find $T_{1/2}^{\text{RMF}} < T_{1/2}^{\text{M3Y}}$ for all the nuclei considered, which is attributed to the fact that M3Y barrier is always higher and wider than the RMF barrier.

In order to intuitively judge the consistency of theoretical calculations and experiments, the logarithms of the ratios of calculated α -decay half-lives to experimental data for the 106 known Ac, Th, Pa, U, Np, and Pu isotopes are plotted in Fig. 2. For comparison, the results from the DDCM-M3Y calculations and the empirical UDL formula are also shown there. In general, the three calculations agree with the experimental data well. Most $\log_{10}(T_{1/2}^{\text{cal}}/T_{1/2}^{\text{exp}})$ values lie between 1 and -1 . Many of them approach zero. A few large deviations appearing in several nuclei may come from the uncertainty of the angular momentum taken away by the α particle. Compared with the empirical UDL formula, the DDCM-RMF and DDCM-M3Y calculations agree with experiment better.

To quantitatively compare the accuracy of the three calculations, we present the standard deviations between the

calculated α -decay half-lives and the experimental data for the 106 known Ac, Th, Pa, U, Np, and Pu isotopes. The standard deviation σ is calculated with the following formula:

$$\sigma = \left[\frac{1}{n-1} \sum_{i=1}^n (\log_{10} T_{1/2}^{\text{cal}} - \log_{10} T_{1/2}^{\text{exp}})^2 \right]^{1/2}. \quad (17)$$

σ is 0.64, 0.57, and 0.94 in the DDCM-RMF calculations, the DDCM-M3Y calculations, and the empirical UDL formula, respectively. These indicate that the DDCM-RMF calculations, the DDCM-M3Y calculations, and the empirical formulas UDL are appropriate to describe the α decay for these neutron-deficient nuclei. Comparably, the α -decay half-lives from the DDCM-RMF calculations and the DDCM-M3Y calculations are in better agreement with experiment. It should be mentioned that the same α -preformation factor is used in calculating the α -decay half-lives in the DDCM-RMF calculations and the DDCM-M3Y calculations.

Since these three models can describe the known α -decays well, especially the DDCM-RMF with more microscopic theoretical foundations, it is meaningful to extend these three models to describe some unknown α decays. Based on the considerations, we calculate the α -decay half-lives for these unknown neutron-deficient nuclei with $89 \leq Z \leq 94$. The binding energies and α decay energies in the calculations are adopted from the WS4+RBF model, which can reproduce well experimental binding energies for known nuclei [66]. The spin and parity values of these nuclei are taken from the calculations of odd-nucleon spin and parity at the nuclear ground state [65]. The calculated results are listed in Table II. Except for the lack of the experimental α -decay half-lives, the other labels are same as those in Table I. Table II shows that the three calculations give almost consistent results, which reflects that the present theoretical predictions are credible.

The α -decay half-lives for the neutron-deficient nuclei with $89 \leq Z \leq 94$ varying with mass number are shown in Fig. 3. To systematically show the evolution of α -decay half-lives with mass number, the results for these known nuclei displayed in Fig. 2 are also included in the figure. The results in the DDCM-RMF calculations, the DDCM-M3Y calculations, and the UDL formula are represented by red hexagons, blue rhombuses, and green squares, respectively. The black spheres represent the experimental data. The α -decay half-lives of unknown nuclei are surrounded by a square box. From Fig. 3(a), it can be seen that these three calculations agree with experiment for the Ac isotopes. The experimental trend of α -decay half-lives with mass number is reproduced well. Comparably, the α -decay half-lives in the DDCM-RMF calculations agree with experiment data better. On the side of $N < 126$, the known neutron-deficient nuclei $^{205-214}\text{Ac}$ have relatively short α -decay half-lives, within about 10^{-2} – 10^0 s, which increase with neutron number. The α -decay half-lives and their variations with neutron number are in good agreement with experiment. Continuing in the neutron-deficient direction to those unknown nuclides $^{201-204}\text{Ac}$, the α -decay half-lives in the three calculations exhibit the same trend, which implies these predicted α -decay half-lives are believable. As the increase of neutron number crosses over the $N = 126$ shell closure, the α -decay half-lives decrease rapidly

TABLE I. (Continued.)

α decay	$J_p^\pi \rightarrow J_d^\pi$	ℓ	Q_α (MeV)	P_α	$T_{1/2}^{\text{exp}}$ (s)	$T_{1/2}^{\text{RMF}}$ (s)	$T_{1/2}^{\text{M3Y}}$ (s)	$T_{1/2}^{\text{UDL}}$ (s)
$^{238}\text{Pu} \rightarrow ^{234}\text{U}$	$0^+ \rightarrow 0^+$	0	5.593	0.145	$2.77 \times 10^{+09}$	$1.74 \times 10^{+09}$	$2.79 \times 10^{+09}$	$1.53 \times 10^{+10}$
$^{239}\text{Pu} \rightarrow ^{235}\text{U}$	$1/2^+ \rightarrow 7/2^-$	3	5.245	0.083	$7.61 \times 10^{+11}$	$1.81 \times 10^{+12}$	$2.36 \times 10^{+12}$	$2.19 \times 10^{+12}$
$^{240}\text{Pu} \rightarrow ^{236}\text{U}$	$0^+ \rightarrow 0^+$	0	5.256	0.129	$2.07 \times 10^{+11}$	$1.90 \times 10^{+11}$	$3.18 \times 10^{+11}$	$1.79 \times 10^{+12}$
$^{242}\text{Pu} \rightarrow ^{238}\text{U}$	$0^+ \rightarrow 0^+$	0	4.984	0.132	$1.18 \times 10^{+13}$	$1.06 \times 10^{+13}$	$1.93 \times 10^{+13}$	$1.17 \times 10^{+14}$
$^{244}\text{Pu} \rightarrow ^{240}\text{U}$	$0^+ \rightarrow 0^+$	0	4.666	0.126	$2.57 \times 10^{+15}$	$2.04 \times 10^{+15}$	$3.88 \times 10^{+15}$	$2.52 \times 10^{+16}$

and reach a minimum 10^{-8} s at $N = 128$. There are relatively large deviations between the calculated α -decay life-times and the experimental data for the nuclei near the neutron magic number $N = 126$, especially in the UDL calculations, which lack consideration of shell effects.

From Figs. 3(b)–3(e), it can be seen that, on the side of $N < 126$, the predicted α -decay half-lives for $^{205-206}\text{Th}$, $^{209-210}\text{Pa}$, and $^{212-213}\text{U}$ are very short, within 10^{-4} – 10^{-3} s, while those for $^{215-218}\text{Np}$ are shorter, within 10^{-5} – 10^{-4} s. With the increase of proton number, the α -decay half-lives become shorter for these neutron-deficient nuclei. In Figs. 3(d) and 3(e), the predicted α -decay life-times for ^{220}U ($N = 128$) and ^{221}Np ($N = 128$) are the shortest, which indicates the

persistence of the $N = 126$ shell closure in the U and Np isotopes. It is worth mentioning that the half-life of the newly synthesized ^{214}U is 0.52 ms, while that in the DDCM-RMF calculations is 0.81 ms, which confirms the reliability of the DDCM-RMF calculations.

In Ref. [7], it was indicated that the shell stability of $N = 126$ weakens towards $Z = 92$, which may be due to the loss of the $Z = 82$ shell closure. It is of great interest to explore whether this weakening effect is enhanced for the higher- Z Pu isotopes. The experimental data on the α -decay support the existence near $N = 126$ of shell closure in the Np isotopes. Therefore, it is necessary to check systematically the $N = 126$ shell weakening towards $Z = 92$. For all the Ac–Np isotopes,

TABLE II. The same as Table I, but for these unknown neutron-deficient nuclei with $89 \leq Z \leq 94$. The α -decay energy Q_α are taken from the WS4+RBF [51]. Except for the lack of experimental α -decay half lives, the labels of the other columns are the same as those in Table I.

α decay	$J_p^\pi \rightarrow J_d^\pi$	ℓ	Q_α (MeV)	P_α	$T_{1/2}^{\text{RMF}}$ (s)	$T_{1/2}^{\text{M3Y}}$ (s)	$T_{1/2}^{\text{UDL}}$ (s)
$Z = 89$							
$^{201}\text{Ac} \rightarrow ^{197}\text{Fr}$	$5/2^- * \rightarrow (7/2^-)$	2	8.476	0.112	6.88×10^{-04}	9.68×10^{-04}	1.69×10^{-04}
$^{202}\text{Ac} \rightarrow ^{198}\text{Fr}$	$3^- * \rightarrow 3^+ \#$	1	8.420	0.035	1.92×10^{-03}	2.80×10^{-03}	2.40×10^{-04}
$^{203}\text{Ac} \rightarrow ^{199}\text{Fr}$	$7/2^- * \rightarrow 1/2^+ \#$	3	8.316	0.099	4.06×10^{-03}	4.28×10^{-03}	4.80×10^{-04}
$^{204}\text{Ac} \rightarrow ^{200}\text{Fr}$	$2^- * \rightarrow (3^+)$	1	8.032	0.020	4.33×10^{-02}	5.20×10^{-02}	3.68×10^{-03}
$Z = 90$							
$^{205}\text{Th} \rightarrow ^{201}\text{Ra}$	$3/2^+ * \rightarrow (3/2^-)$	1	8.530	0.098	5.80×10^{-04}	9.15×10^{-04}	2.58×10^{-04}
$^{206}\text{Th} \rightarrow ^{202}\text{Ra}$	$0^+ \rightarrow 0^+$	0	8.434	0.217	3.60×10^{-04}	5.70×10^{-04}	4.86×10^{-04}
$Z = 91$							
$^{209}\text{Pa} \rightarrow ^{205}\text{Ac}$	$5/2^- * \rightarrow 9/2^-$	2	8.663	0.100	8.18×10^{-04}	1.27×10^{-03}	2.28×10^{-04}
$^{210}\text{Pa} \rightarrow ^{206}\text{Ac}$	$0^- * \rightarrow 3^+$	3	8.749	0.043	2.01×10^{-03}	2.98×10^{-03}	1.22×10^{-04}
$Z = 92$							
$^{212}\text{U} \rightarrow ^{208}\text{Th}$	$0^+ \rightarrow 0^+$	0	8.707	0.240	2.34×10^{-04}	3.48×10^{-04}	3.87×10^{-04}
$^{213}\text{U} \rightarrow ^{209}\text{Th}$	$1/2^- * \rightarrow 5/2^- \#$	2	8.669	0.102	1.74×10^{-03}	2.05×10^{-03}	4.83×10^{-04}
$^{220}\text{U} \rightarrow ^{216}\text{Th}$	$0^+ \rightarrow 0^+$	0	10.479	0.258	2.00×10^{-08}	3.13×10^{-08}	6.81×10^{-09}
$Z = 93$							
$^{215}\text{Np} \rightarrow ^{211}\text{Pa}$	$11/2^+ * \rightarrow 9/2^-$	1	9.393	0.110	2.22×10^{-05}	3.77×10^{-05}	9.70×10^{-06}
$^{216}\text{Np} \rightarrow ^{212}\text{Pa}$	$4^- * \rightarrow 3^+ \#$	1	9.031	0.037	5.40×10^{-04}	9.87×10^{-04}	9.47×10^{-05}
$^{217}\text{Np} \rightarrow ^{213}\text{Pa}$	$11/2^+ * \rightarrow 9/2^-$	1	8.917	0.112	3.49×10^{-04}	6.96×10^{-04}	1.94×10^{-04}
$^{218}\text{Np} \rightarrow ^{214}\text{Pa}$	$6^- * \rightarrow 7^+ \#$	1	9.142	0.040	2.47×10^{-04}	3.38×10^{-04}	4.22×10^{-05}
$^{221}\text{Np} \rightarrow ^{217}\text{Pa}$	$1/2^+ * \rightarrow 9/2^-$	5	10.567	0.144	1.85×10^{-08}	3.04×10^{-08}	9.50×10^{-09}
$Z = 94$							
$^{220}\text{Pu} \rightarrow ^{216}\text{U}$	$0^+ \rightarrow 0^+$	0	9.494	0.240	7.22×10^{-06}	1.15×10^{-05}	1.04×10^{-05}
$^{221}\text{Pu} \rightarrow ^{217}\text{U}$	$9/2^+ * \rightarrow 1/2^- \#$	5	10.109	0.130	1.04×10^{-05}	1.10×10^{-05}	2.65×10^{-07}
$^{222}\text{Pu} \rightarrow ^{218}\text{U}$	$0^+ \rightarrow 0^+$	0	10.772	0.277	7.49×10^{-09}	1.37×10^{-08}	7.22×10^{-09}
$^{223}\text{Pu} \rightarrow ^{219}\text{U}$	$3/2^+ * \rightarrow 9/2^+ \#$	4	10.340	0.142	7.73×10^{-07}	9.47×10^{-07}	6.79×10^{-08}
$^{224}\text{Pu} \rightarrow ^{220}\text{U}$	$0^+ \rightarrow 0^+$	0	9.796	0.251	8.82×10^{-07}	1.22×10^{-06}	1.43×10^{-06}
$^{225}\text{Pu} \rightarrow ^{221}\text{U}$	$1/2^+ * \rightarrow 9/2^+ \#$	4	9.377	0.129	1.55×10^{-04}	1.83×10^{-04}	1.77×10^{-05}
$^{226}\text{Pu} \rightarrow ^{222}\text{U}$	$0^+ \rightarrow 0^+$	0	8.915	0.230	1.85×10^{-04}	2.07×10^{-04}	3.51×10^{-04}
$^{227}\text{Pu} \rightarrow ^{223}\text{U}$	$3/2^+ * \rightarrow 7/2^+ \#$	2	8.569	0.116	6.12×10^{-03}	7.57×10^{-03}	3.82×10^{-03}

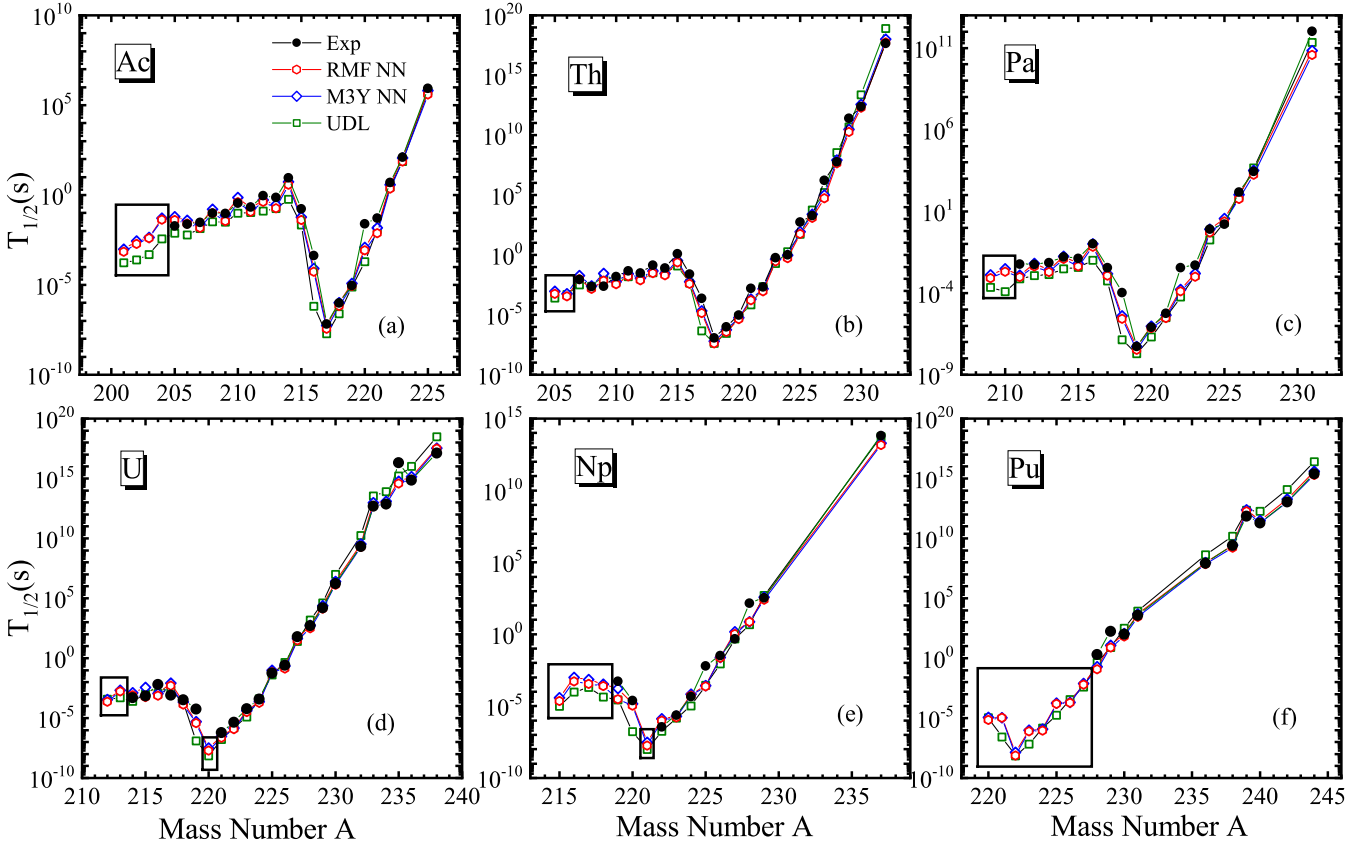


FIG. 3. The calculated α -decay half-lives and their comparison with experiment. The results from the DDCM-RMF calculations, the DDCM-M3Y calculations, and the empirical UDL formula are denoted by red hexagons, blue rhombuses, and green squares, respectively. The experimental data is marked as black spheres. Panels (a), (b), (c), (d), (e), and (f) show the results for the Ac, Th, Pa, U, Np, and Pu isotopes, respectively. Results for the unknown isotopes are enclosed in a box.

the calculations indicates that the nuclei with $N = 128$ have the shortest α -decay half-life. The same case appears in the higher- Z Pu isotopes: the Pu nucleus with $N = 128$ has the shortest α -decay half-life. Compared with the Ac–Np isotopes, the $N = 126$ shell closure remains solidly in the $Z = 94$ isotopes.

To gain insight into the evolution of $N = 126$ shell closure of in the Pu isotopes, we analyze the systematic behavior of the α -preformation factor around $N = 126$. Considering the odd-even differences, we discuss the preformation factor for even-even, even-odd, odd-even, and odd-odd nuclei, respectively. The calculated preformation factor P_α and the extracted Q_α are shown in Fig. 4 for these neutron-deficient nuclei with $89 \leq Z \leq 94$. In general, there are $P_\alpha^{\text{even-even}} > P_\alpha^{\text{odd-A}} > P_\alpha^{\text{odd-odd}}$. For the odd- A nuclei, due to the Pauli blocking effect, a single unpaired nucleon hinders the formation of α particle, resulting in a decrease in the preformation factor. For the odd-odd nuclei, due to the existence of two unpaired nucleons in the nucleus, this hindering effect is more significant, and the preformation factor of odd-odd nuclei is further reduced. For the Ac, Th, Pa, and U isotopes, the preformation factor decreases with the increase of neutron number on the side of $N < 126$. The preformation factor reaches a minimum value at the shell closure at $N = 126$. After crossing over the $N = 126$ shell, the magnitude of

α -preformation factor increases significantly and reaches a maximum value at $N = 128$. After crossing over the $N = 128$ shell, the preformation factor decreases with the increase of neutron number. The typical decrease in P_α is caused by the stabilizing effect of the $N = 126$ neutron-shell closure. This shell effect leads to a significant increase of P_α at $N = 128$. Clustering is enhanced when two loosely bound neutrons above the $N = 126$ shell participate in the formation of α clusters. For the Np and Pu isotopes, the sharp increase of P_α from $N = 126$ to $N = 128$ is also the consequence of shell effects. These indicate that the preformation factor shows clearly the $N = 126$ shell effect for the neutron-deficient nuclei considered here. A few irregularities in the variations of P_α in the Ac–Pu isotopes are mainly due to the presence of unpaired nucleons masking the effects caused by the shell effect. For the Ac–Pu isotopes with even neutron number, the behavior of Q_α as a function of neutron number is almost identical to that of P_α , which provides further evidence for the $N = 126$ shell effect in neutron-deficient nuclei. It is further confirmed that the $N = 126$ shell closure remains solidly in the Pu isotopes beyond $Z = 92$. Unlike the nuclei with even neutron number, since there is no magic number $N = 126$, the variation of preformation factor with neutron number in the nuclei with odd neutron number is rather complicated.

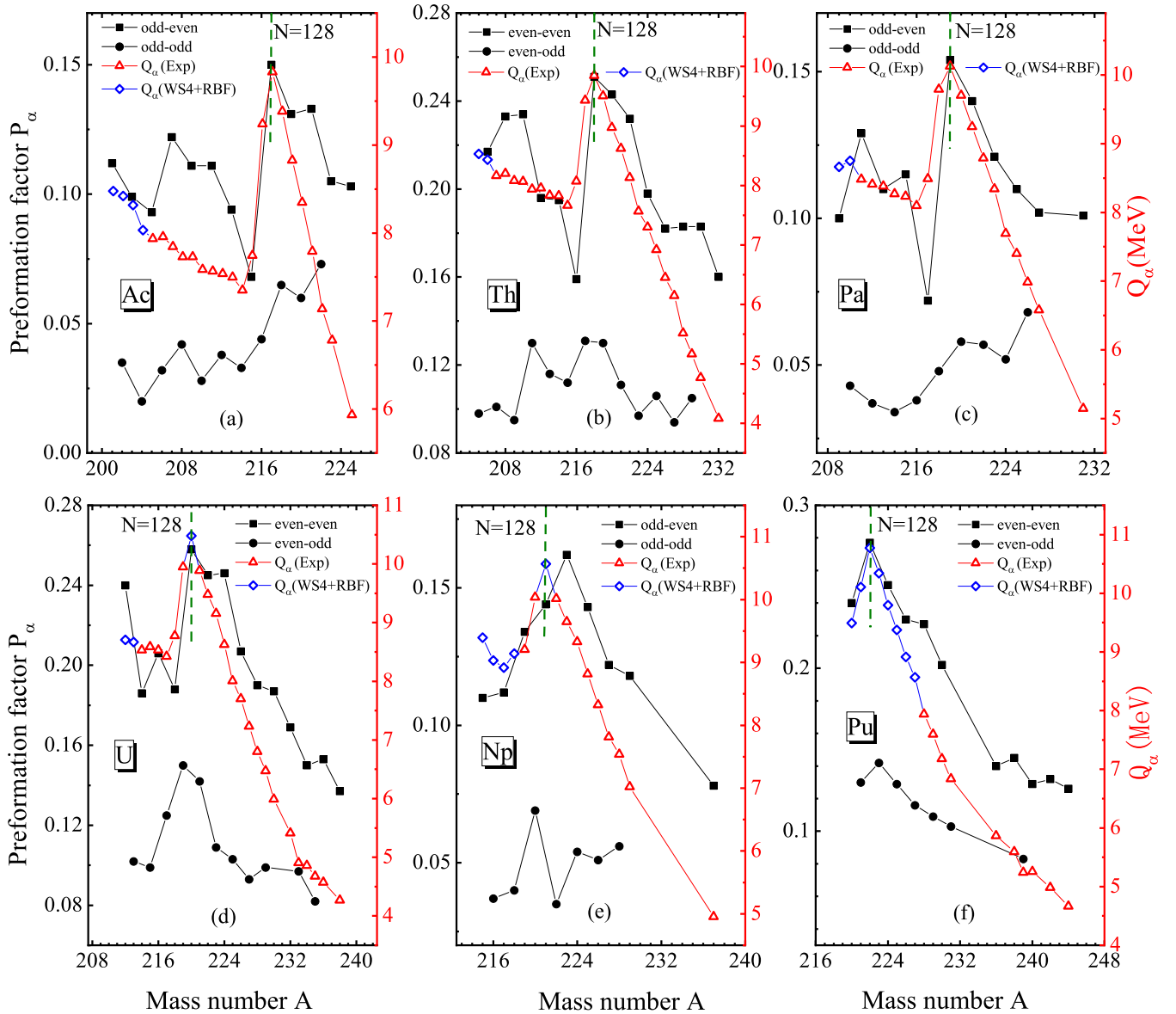


FIG. 4. The α -preformation factor P_α and its variation with mass number for the even-even, even-odd, odd-even, and odd-odd nuclei. The decay energy Q_α of α decay in atomic nuclei and its variation with mass number. The results for the Ac, Th, Pa, U, Np, and Pu isotopes are displayed in panels (a), (b), (c), (d), (e), and (f), respectively.

For the convenience of experimental reference, in Table III we have listed the α -decay half-lives for all the predicted neutron-deficient α -decay chains. The first column is the specified α -decay chain. The second column gives the spin and parity of the parent and daughter nuclei, respectively, which are taken from Refs. [48,65]. The third column is the angular momentum taken away by the α particle. The fourth column gives the decay energy of the α particle, Q_α , which is obtained from the WS4+RBF model for unknown nuclei and from the experimental data in the AME2020 for known nuclei. The fifth column is the α -preformation factor calculated with the cluster formation model. The calculated α -decay half-lives in the DDCM-RMF calculations, the DDCM-M3Y calculations, and the empirical UDL formula are shown in the sixth, seventh, and eighth columns, respectively. There are 4α chains in the isotopes $^{201-204}\text{Ac}$, $^{205-206}\text{Th}$, and $^{209-210}\text{Pa}$, and 5α chains

in these isotopes $^{212-213,220}\text{U}$, $^{215-218,221}\text{Np}$, and $^{220-227}\text{Pu}$. For these predicted neutron-deficient nuclei, their decay energies and products decrease, while their half-lives increase along the corresponding α -decay chains. This result can guide experiments to detect neutron-deficient nuclei.

IV. SUMMARY

The DDCM combined with RMF is used to investigate the structure and decay for the neutron-deficient nuclei with $89 \leq Z \leq 94$. The nucleon-nucleon interactions and matter density distributions from the RMF calculations are used to construct the α -daughter potential with the double-folding model. For convenience, the model is called DDCM-RMF. For comparison, a widely used M3Y-Paris nucleon-nucleon interaction is used instead of the interaction from RMF; this

TABLE III. The α -decay half lives of these α -decay chains for the neutron-deficient nuclei with $89 \leq Z \leq 94$. The first column indicates the specific α -decay chain. The labels for the other columns are the same as those in Table II.

α decay	$j_p^\pi \rightarrow j_d^\pi$	ℓ	Q_α (MeV)	P_α	$T_{1/2}^{\text{RMF}}$ (s)	$T_{1/2}^{\text{M3Y}}$ (s)	$T_{1/2}^{\text{UDL}}$ (s)
$Z = 89$							
$^{201}\text{Ac} \rightarrow ^{197}\text{Fr}$	$5/2^-_* \rightarrow (7/2^-)$	2	8.476	0.112	6.88×10^{-04}	9.68×10^{-04}	1.69×10^{-04}
$^{197}\text{Fr} \rightarrow ^{193}\text{At}$	$(7/2^-) \rightarrow 1/2^+$	3	7.896	0.112	1.32×10^{-02}	1.70×10^{-02}	1.83×10^{-03}
$^{193}\text{At} \rightarrow ^{189}\text{Bi}$	$1/2^+ \rightarrow 9/2^-$	5	7.572	0.136	1.42×10^{-01}	1.50×10^{-01}	3.36×10^{-03}
$^{189}\text{Bi} \rightarrow ^{185}\text{Tl}$	$9/2^- \rightarrow 1/2^+$	5	7.268	0.145	2.25×10^{-01}	2.28×10^{-01}	5.49×10^{-03}
$^{202}\text{Ac} \rightarrow ^{198}\text{Fr}$	$3^-_* \rightarrow 3^+\#$	1	8.420	0.035	1.92×10^{-03}	2.80×10^{-03}	2.40×10^{-04}
$^{198}\text{Fr} \rightarrow ^{194}\text{At}$	$3^+\# \rightarrow (5^-)$	3	7.869	0.038	4.59×10^{-02}	5.69×10^{-02}	2.15×10^{-03}
$^{194}\text{At} \rightarrow ^{190}\text{Bi}$	$(5^-) \rightarrow (3^+)$	3	7.454	0.034	2.07×10^{-01}	2.17×10^{-01}	8.20×10^{-03}
$^{190}\text{Bi} \rightarrow ^{186}\text{Tl}$	$(3^+) \rightarrow (2^-)$	4	6.862	0.044	$6.68 \times 10^{+00}$	$7.62 \times 10^{+00}$	1.65×10^{-01}
$^{203}\text{Ac} \rightarrow ^{199}\text{Fr}$	$7/2^-_* \rightarrow 1/2^+\#$	3	8.316	0.099	4.06×10^{-03}	4.28×10^{-03}	4.80×10^{-04}
$^{199}\text{Fr} \rightarrow ^{195}\text{At}$	$1/2^+\# \rightarrow 1/2^+$	0	7.817	0.133	3.71×10^{-03}	7.22×10^{-03}	3.07×10^{-03}
$^{195}\text{At} \rightarrow ^{191}\text{Bi}$	$1/2^+ \rightarrow 9/2^-$	5	7.344	0.137	4.95×10^{-01}	6.35×10^{-01}	1.92×10^{-02}
$^{191}\text{Bi} \rightarrow ^{187}\text{Tl}$	$9/2^- \rightarrow 1/2^+$	5	6.780	0.145	$7.67 \times 10^{+00}$	$1.15 \times 10^{+01}$	3.29×10^{-01}
$^{204}\text{Ac} \rightarrow ^{200}\text{Fr}$	$2^-_* \rightarrow (3^+)$	1	8.032	0.020	4.33×10^{-02}	5.20×10^{-02}	3.68×10^{-03}
$^{200}\text{Fr} \rightarrow ^{196}\text{At}$	$(3^+) \rightarrow (3^+)$	0	7.622	0.031	6.45×10^{-02}	1.15×10^{-01}	1.34×10^{-02}
$^{196}\text{At} \rightarrow ^{192}\text{Bi}$	$(3^+) \rightarrow (3^+)$	0	7.196	0.034	2.55×10^{-01}	3.93×10^{-01}	6.31×10^{-02}
$^{192}\text{Bi} \rightarrow ^{188}\text{Tl}$	$(3^+) \rightarrow 2^- \#$	1	6.377	0.041	$5.63 \times 10^{+01}$	$8.77 \times 10^{+01}$	$1.42 \times 10^{+01}$
$Z = 90$							
$^{205}\text{Th} \rightarrow ^{201}\text{Ra}$	$3/2^+_* \rightarrow (3/2^-)$	1	8.530	0.098	5.80×10^{-04}	9.15×10^{-04}	2.58×10^{-04}
$^{201}\text{Ra} \rightarrow ^{197}\text{Rn}$	$(3/2^-) \rightarrow 3/2^-$	0	8.002	0.126	2.63×10^{-03}	4.16×10^{-03}	1.92×10^{-03}
$^{197}\text{Rn} \rightarrow ^{193}\text{Po}$	$3/2^- \rightarrow 3/2^-$	0	7.411	0.121	3.41×10^{-02}	5.39×10^{-02}	2.94×10^{-02}
$^{193}\text{Po} \rightarrow ^{189}\text{Pb}$	$3/2^- \rightarrow 3/2^-$	0	7.094	0.111	1.02×10^{-01}	1.32×10^{-01}	5.78×10^{-02}
$^{206}\text{Th} \rightarrow ^{202}\text{Ra}$	$0^+ \rightarrow 0^+$	0	8.434	0.217	3.60×10^{-04}	5.70×10^{-04}	4.86×10^{-04}
$^{202}\text{Ra} \rightarrow ^{198}\text{Rn}$	$0^+ \rightarrow 0^+$	0	7.880	0.248	3.14×10^{-03}	4.81×10^{-03}	4.62×10^{-03}
$^{198}\text{Rn} \rightarrow ^{194}\text{Po}$	$0^+ \rightarrow 0^+$	0	7.349	0.239	2.68×10^{-02}	4.37×10^{-02}	4.69×10^{-02}
$^{194}\text{Po} \rightarrow ^{190}\text{Pb}$	$0^+ \rightarrow 0^+$	0	6.987	0.235	1.04×10^{-01}	1.45×10^{-01}	1.40×10^{-01}
$Z = 91$							
$^{209}\text{Pa} \rightarrow ^{205}\text{Ac}$	$5/2^-_* \rightarrow 9/2^-$	2	8.663	0.100	8.18×10^{-04}	1.27×10^{-03}	2.28×10^{-04}
$^{205}\text{Ac} \rightarrow ^{201}\text{Fr}$ [1]	$9/2^- \rightarrow 9/2^-$	0	7.935	0.093	4.08×10^{-02}	6.24×10^{-02}	7.38×10^{-03}
$^{201}\text{Fr} \rightarrow ^{197}\text{At}$	$9/2^- \rightarrow 9/2^-$	0	7.519	0.126	3.42×10^{-02}	5.70×10^{-02}	2.95×10^{-02}
$^{197}\text{At} \rightarrow ^{193}\text{Bi}$	$9/2^- \rightarrow 9/2^-$	0	7.104	0.129	1.37×10^{-01}	2.16×10^{-01}	1.33×10^{-01}
$^{210}\text{Pa} \rightarrow ^{206}\text{Ac}$	$0^-_* \rightarrow 3^+$	3	8.749	0.043	2.01×10^{-03}	2.98×10^{-03}	1.22×10^{-04}
$^{206}\text{Ac} \rightarrow ^{202}\text{Fr}$	$3^+ \rightarrow 3^+$	0	7.958	0.032	2.56×10^{-02}	3.98×10^{-02}	5.94×10^{-03}
$^{202}\text{Fr} \rightarrow ^{198}\text{At}$	$3^+ \rightarrow 3^+$	0	7.385	0.036	3.33×10^{-01}	5.38×10^{-01}	8.52×10^{-02}
$^{198}\text{At} \rightarrow ^{194}\text{Bi}$	$3^+ \rightarrow 3^+$	0	6.889	0.038	$2.69 \times 10^{+00}$	$4.26 \times 10^{+00}$	8.50×10^{-01}
$Z = 92$							
$^{212}\text{U} \rightarrow ^{208}\text{Th}$	$0^+ \rightarrow 0^+$	0	8.707	0.240	2.34×10^{-04}	3.48×10^{-04}	3.87×10^{-04}
$^{208}\text{Th} \rightarrow ^{204}\text{Ra}$	$0^+ \rightarrow 0^+$	0	8.202	0.233	1.47×10^{-03}	2.49×10^{-03}	2.39×10^{-03}
$^{204}\text{Ra} \rightarrow ^{200}\text{Rn}$	$0^+ \rightarrow 0^+$	0	7.637	0.231	2.80×10^{-02}	2.91×10^{-02}	2.85×10^{-02}
$^{200}\text{Rn} \rightarrow ^{196}\text{Po}$	$0^+ \rightarrow 0^+$	0	7.043	0.221	3.28×10^{-01}	5.68×10^{-01}	5.94×10^{-01}
$^{196}\text{Po} \rightarrow ^{192}\text{Pb}$	$0^+ \rightarrow 0^+$	0	6.658	0.216	$1.65 \times 10^{+00}$	$2.07 \times 10^{+00}$	$2.53 \times 10^{+00}$
$^{213}\text{U} \rightarrow ^{209}\text{Th}$	$1/2^-_* \rightarrow 5/2^- \#$	2	8.669	0.102	1.74×10^{-03}	2.05×10^{-03}	4.83×10^{-04}
$^{209}\text{Th} \rightarrow ^{205}\text{Ra}$	$5/2^- \# \rightarrow 3/2^-$	2	8.080	0.095	7.39×10^{-03}	2.77×10^{-02}	5.69×10^{-03}
$^{205}\text{Ra} \rightarrow ^{201}\text{Rn}$	$3/2^- \rightarrow 3/2^-$	0	7.486	0.111	1.27×10^{-01}	1.52×10^{-01}	6.52×10^{-01}
$^{201}\text{Rn} \rightarrow ^{197}\text{Po}$	$3/2^- \rightarrow (3/2^-)$	0	6.861	0.097	$3.43 \times 10^{+00}$	$6.35 \times 10^{+00}$	$2.31 \times 10^{+01}$
$^{197}\text{Po} \rightarrow ^{193}\text{Pb}$	$(3/2^-) \rightarrow 3/2^- \#$	0	6.411	0.086	$3.89 \times 10^{+01}$	$4.83 \times 10^{+01}$	$2.63 \times 10^{+01}$
$^{220}\text{U} \rightarrow ^{216}\text{Th}$	$0^+ \rightarrow 0^+$	0	10.479	0.258	2.00×10^{-08}	3.13×10^{-08}	6.81×10^{-09}
$^{216}\text{Th} \rightarrow ^{212}\text{Ra}$	$0^+ \rightarrow 0^+$	0	8.072	0.159	3.78×10^{-03}	5.88×10^{-03}	4.56×10^{-03}
$^{212}\text{Ra} \rightarrow ^{208}\text{Rn}$	$0^+ \rightarrow 0^+$	0	7.042	0.171	$2.11 \times 10^{+00}$	$3.03 \times 10^{+00}$	$3.28 \times 10^{+00}$
$^{208}\text{Rn} \rightarrow ^{204}\text{Po}$	$0^+ \rightarrow 0^+$	0	6.261	0.163	$3.94 \times 10^{+02}$	$5.96 \times 10^{+02}$	$8.17 \times 10^{+02}$
$^{204}\text{Po} \rightarrow ^{200}\text{Pb}$	$0^+ \rightarrow 0^+$	0	5.485	0.158	$2.65 \times 10^{+05}$	$4.56 \times 10^{+05}$	$6.13 \times 10^{+05}$

TABLE III. (Continued.)

α decay	$J_p^\pi \rightarrow J_d^\pi$	ℓ	Q_α (MeV)	P_α	$T_{1/2}^{\text{RMF}}$ (s)	$T_{1/2}^{\text{M3Y}}$ (s)	$T_{1/2}^{\text{UDL}}$ (s)
$Z = 93$							
$^{215}\text{Np} \rightarrow ^{211}\text{Pa}$	$11/2^+ * \rightarrow 9/2^-$	1	9.393	0.110	2.22×10^{-05}	3.77×10^{-05}	9.70×10^{-06}
$^{211}\text{Pa} \rightarrow ^{207}\text{Ac}$	$9/2^- \rightarrow 9/2^-$	0	8.481	0.129	9.60×10^{-04}	1.21×10^{-03}	7.48×10^{-04}
$^{207}\text{Ac} \rightarrow ^{203}\text{Fr}$	$9/2^- \rightarrow 9/2^-$	0	7.845	0.122	1.47×10^{-02}	2.32×10^{-02}	1.36×10^{-02}
$^{203}\text{Fr} \rightarrow ^{199}\text{At}$	$9/2^- \rightarrow 9/2^-$	0	7.275	0.118	2.42×10^{-01}	3.79×10^{-01}	2.07×10^{-01}
$^{199}\text{At} \rightarrow ^{195}\text{Bi}$	$9/2^- \rightarrow 9/2^-$	0	6.777	0.119	$2.20 \times 10^{+00}$	$3.57 \times 10^{+00}$	$2.27 \times 10^{+00}$
$^{216}\text{Np} \rightarrow ^{212}\text{Pa}$	$4^- * \rightarrow 3^+ \#$	1	9.031	0.037	5.40×10^{-04}	9.87×10^{-04}	9.47×10^{-05}
$^{212}\text{Pa} \rightarrow ^{208}\text{Ac}$	$3^+ \# \rightarrow 3^+$	0	8.411	0.037	4.41×10^{-03}	6.50×10^{-03}	1.18×10^{-03}
$^{208}\text{Ac} \rightarrow ^{204}\text{Fr}$	$3^+ \rightarrow 3^+$	0	7.729	0.042	9.60×10^{-02}	1.58×10^{-01}	3.26×10^{-02}
$^{204}\text{Fr} \rightarrow ^{200}\text{At}$	$3^+ \rightarrow (3^+)$	0	7.170	0.042	$1.64 \times 10^{+00}$	$2.40 \times 10^{+00}$	4.90×10^{-01}
$^{200}\text{At} \rightarrow ^{196}\text{Bi}$	$(3^+) \rightarrow (3^+)$	0	6.596	0.042	$3.08 \times 10^{+01}$	$5.03 \times 10^{+01}$	$1.20 \times 10^{+01}$
$^{217}\text{Np} \rightarrow ^{213}\text{Pa}$	$11/2^+ * \rightarrow 9/2^-$	1	8.917	0.112	3.49×10^{-04}	6.96×10^{-04}	1.94×10^{-04}
$^{213}\text{Pa} \rightarrow ^{209}\text{Ac}$	$9/2^- \rightarrow 9/2^-$	0	8.384	0.110	1.93×10^{-03}	2.55×10^{-03}	1.38×10^{-03}
$^{209}\text{Ac} \rightarrow ^{205}\text{Fr}$	$9/2^- \rightarrow 9/2^-$	0	7.730	0.111	3.51×10^{-02}	7.29×10^{-02}	3.11×10^{-02}
$^{205}\text{Fr} \rightarrow ^{201}\text{At}$	$9/2^- \rightarrow 9/2^-$	0	7.055	0.116	$1.69 \times 10^{+00}$	$1.77 \times 10^{+00}$	$1.30 \times 10^{+00}$
$^{201}\text{At} \rightarrow ^{197}\text{Bi}$	$9/2^- \rightarrow 9/2^-$	0	6.473	0.114	$3.43 \times 10^{+01}$	$5.91 \times 10^{+01}$	$3.85 \times 10^{+01}$
$^{218}\text{Np} \rightarrow ^{214}\text{Pa}$	$6^- * \rightarrow 7^+ \#$	1	9.142	0.040	2.47×10^{-04}	3.38×10^{-04}	4.22×10^{-05}
$^{214}\text{Pa} \rightarrow ^{210}\text{Ac}$	$7^+ \# \rightarrow 7^+ \#$	0	8.271	0.034	1.24×10^{-02}	1.73×10^{-02}	3.02×10^{-03}
$^{210}\text{Ac} \rightarrow ^{206}\text{Fr}$	$7^+ \# \rightarrow 3^+$	4	7.586	0.028	4.02×10^{-01}	7.11×10^{-01}	9.55×10^{-02}
$^{206}\text{Fr} \rightarrow ^{202}\text{At}$	$3^+ \rightarrow 3^+$	0	6.923	0.027	$1.71 \times 10^{+01}$	$2.29 \times 10^{+01}$	$4.11 \times 10^{+00}$
$^{202}\text{At} \rightarrow ^{198}\text{Bi}$	$3^+ \rightarrow 3^+$	0	6.354	0.028	$4.21 \times 10^{+02}$	$8.59 \times 10^{+02}$	$1.22 \times 10^{+02}$
$^{221}\text{Np} \rightarrow ^{217}\text{Pa}$	$1/2^+ * \rightarrow 9/2^-$	5	10.567	0.144	1.85×10^{-08}	3.04×10^{-08}	9.50×10^{-09}
$^{217}\text{Pa} \rightarrow ^{213}\text{Ac}$	$9/2^- \rightarrow 9/2^-$	0	8.489	0.072	1.15×10^{-03}	1.50×10^{-03}	5.55×10^{-04}
$^{213}\text{Ac} \rightarrow ^{209}\text{Fr}$	$9/2^- \rightarrow 9/2^-$	0	7.498	0.094	1.87×10^{-01}	2.93×10^{-01}	1.75×10^{-01}
$^{209}\text{Fr} \rightarrow ^{205}\text{At}$	$9/2^- \rightarrow 9/2^-$	0	6.777	0.093	$1.40 \times 10^{+01}$	$2.33 \times 10^{+01}$	$1.42 \times 10^{+01}$
$^{205}\text{At} \rightarrow ^{201}\text{Bi}$	$9/2^- \rightarrow 9/2^-$	0	6.020	0.095	$3.43 \times 10^{+03}$	$5.36 \times 10^{+03}$	$3.76 \times 10^{+03}$
$Z = 94$							
$^{220}\text{Pu} \rightarrow ^{216}\text{U}$	$0^+ \rightarrow 0^+$	0	9.494	0.240	7.22×10^{-06}	1.15×10^{-05}	1.04×10^{-05}
$^{216}\text{U} \rightarrow ^{212}\text{Th}$	$0^+ \rightarrow 0^+$	0	8.531	0.206	7.44×10^{-04}	1.16×10^{-03}	1.13×10^{-03}
$^{212}\text{Th} \rightarrow ^{208}\text{Ra}$	$0^+ \rightarrow 0^+$	0	7.958	0.196	7.57×10^{-03}	1.16×10^{-02}	1.28×10^{-02}
$^{208}\text{Ra} \rightarrow ^{204}\text{Rn}$	$0^+ \rightarrow 0^+$	0	7.273	0.196	2.76×10^{-01}	4.45×10^{-01}	5.00×10^{-01}
$^{204}\text{Rn} \rightarrow ^{200}\text{Po}$	$0^+ \rightarrow 0^+$	0	6.547	0.191	$2.79 \times 10^{+01}$	$4.45 \times 10^{+01}$	$5.18 \times 10^{+01}$
$^{221}\text{Pu} \rightarrow ^{217}\text{U}$	$9/2^+ * \rightarrow 1/2^- \#$	5	10.109	0.130	1.04×10^{-05}	1.10×10^{-05}	2.65×10^{-07}
$^{217}\text{U} \rightarrow ^{213}\text{Th}$	$1/2^- \# \rightarrow 5/2^-$	2	8.426	0.125	5.02×10^{-03}	8.37×10^{-03}	2.30×10^{-03}
$^{213}\text{Th} \rightarrow ^{209}\text{Ra}$	$5/2^- \rightarrow 5/2^-$	0	7.837	0.116	3.05×10^{-02}	4.58×10^{-02}	3.15×10^{-02}
$^{209}\text{Ra} \rightarrow ^{205}\text{Rn}$	$5/2^- \rightarrow 5/2^-$	0	7.143	0.103	$1.47 \times 10^{+00}$	$2.46 \times 10^{+00}$	$1.50 \times 10^{+00}$
$^{205}\text{Rn} \rightarrow ^{201}\text{Po}$	$5/2^- \rightarrow 3/2^-$	2	6.386	0.092	$5.88 \times 10^{+02}$	$8.84 \times 10^{+02}$	$2.51 \times 10^{+02}$
$^{222}\text{Pu} \rightarrow ^{218}\text{U}$	$0^+ \rightarrow 0^+$	0	10.772	0.277	7.49×10^{-09}	1.37×10^{-08}	7.22×10^{-09}
$^{218}\text{U} \rightarrow ^{214}\text{Th}$	$0^+ \rightarrow 0^+$	0	8.775	0.188	1.34×10^{-04}	2.18×10^{-04}	1.90×10^{-04}
$^{214}\text{Th} \rightarrow ^{210}\text{Ra}$	$0^+ \rightarrow 0^+$	0	7.827	0.195	2.00×10^{-02}	2.88×10^{-02}	3.28×10^{-02}
$^{210}\text{Ra} \rightarrow ^{206}\text{Rn}$	$0^+ \rightarrow 0^+$	0	7.151	0.187	7.44×10^{-01}	$1.43 \times 10^{+00}$	$1.34 \times 10^{+00}$
$^{206}\text{Rn} \rightarrow ^{202}\text{Po}$	$0^+ \rightarrow 0^+$	0	6.384	0.180	$1.55 \times 10^{+02}$	$1.68 \times 10^{+02}$	$2.46 \times 10^{+02}$
$^{223}\text{Pu} \rightarrow ^{219}\text{U}$	$3/2^+ * \rightarrow 9/2^+ \#$	4	10.340	0.142	7.73×10^{-07}	9.47×10^{-07}	6.79×10^{-08}
$^{219}\text{U} \rightarrow ^{215}\text{Th}$	$9/2^+ \# \rightarrow (1/2^-)$	5	9.950	0.150	3.84×10^{-06}	5.10×10^{-06}	1.25×10^{-07}
$^{215}\text{Th} \rightarrow ^{211}\text{Ra}$	$(1/2^-) \rightarrow 5/2^-$	2	7.665	0.112	2.35×10^{-01}	3.42×10^{-01}	1.16×10^{-01}
$^{211}\text{Ra} \rightarrow ^{207}\text{Rn}$	$5/2^- \rightarrow 5/2^-$	0	7.042	0.101	$3.35 \times 10^{+00}$	$6.04 \times 10^{+00}$	$3.42 \times 10^{+00}$
$^{207}\text{Rn} \rightarrow ^{203}\text{Po}$	$5/2^- \rightarrow 5/2^-$	0	6.251	0.090	$1.06 \times 10^{+03}$	$1.22 \times 10^{+03}$	$9.44 \times 10^{+02}$
$^{224}\text{Pu} \rightarrow ^{220}\text{U}$	$0^+ \rightarrow 0^+$	0	9.796	0.251	8.82×10^{-07}	1.22×10^{-06}	1.43×10^{-06}
$^{220}\text{U} \rightarrow ^{216}\text{Th}$	$0^+ \rightarrow 0^+$	0	10.479	0.258	2.00×10^{-08}	3.13×10^{-08}	6.81×10^{-09}
$^{216}\text{Th} \rightarrow ^{212}\text{Ra}$	$0^+ \rightarrow 0^+$	0	8.072	0.159	3.78×10^{-03}	5.88×10^{-03}	4.56×10^{-03}
$^{212}\text{Ra} \rightarrow ^{208}\text{Rn}$	$0^+ \rightarrow 0^+$	0	7.032	0.171	$2.11 \times 10^{+00}$	$3.03 \times 10^{+00}$	$3.60 \times 10^{+00}$
$^{208}\text{Rn} \rightarrow ^{204}\text{Po}$	$0^+ \rightarrow 0^+$	0	6.261	0.163	$3.94 \times 10^{+02}$	$5.96 \times 10^{+02}$	$8.17 \times 10^{+02}$

TABLE III. (Continued.)

α decay	$J_p^\pi \rightarrow J_d^\pi$	ℓ	Q_α (MeV)	P_α	$T_{1/2}^{\text{RMF}}$ (s)	$T_{1/2}^{\text{M3Y}}$ (s)	$T_{1/2}^{\text{UDL}}$ (s)
$^{225}\text{Pu} \rightarrow ^{221}\text{U}$	$1/2^+_* \rightarrow 9/2^+\#$	4	9.377	0.129	1.55×10^{-04}	1.83×10^{-04}	1.77×10^{-05}
$^{221}\text{U} \rightarrow ^{217}\text{Th}$	$9/2^+\# \rightarrow 9/2^+\#$	0	9.889	0.142	2.36×10^{-07}	3.01×10^{-07}	1.64×10^{-07}
$^{217}\text{Th} \rightarrow ^{213}\text{Ra}$	$9/2^+\# \rightarrow 1/2^-$	5	9.435	0.131	1.37×10^{-05}	2.06×10^{-05}	4.65×10^{-07}
$^{213}\text{Ra} \rightarrow ^{209}\text{Rn}$	$1/2^- \rightarrow 5/2^-$	2	6.862	0.096	$3.54 \times 10^{+01}$	$4.43 \times 10^{+01}$	$1.66 \times 10^{+01}$
$^{209}\text{Rn} \rightarrow ^{205}\text{Po}$	$5/2^- \rightarrow 5/2^-$	0	6.155	0.083	$2.17 \times 10^{+03}$	$3.38 \times 10^{+03}$	$2.44 \times 10^{+03}$
$^{226}\text{Pu} \rightarrow ^{222}\text{U}$	$0^+ \rightarrow 0^+$	0	8.915	0.230	1.85×10^{-04}	2.07×10^{-04}	3.51×10^{-04}
$^{222}\text{U} \rightarrow ^{218}\text{Th}$	$0^+ \rightarrow 0^+$	0	9.481	0.245	1.16×10^{-06}	1.50×10^{-06}	1.73×10^{-06}
$^{218}\text{Th} \rightarrow ^{214}\text{Ra}$	$0^+ \rightarrow 0^+$	0	9.849	0.251	4.08×10^{-08}	6.14×10^{-08}	4.07×10^{-08}
$^{214}\text{Ra} \rightarrow ^{210}\text{Rn}$	$0^+ \rightarrow 0^+$	0	7.273	0.138	2.98×10^{-01}	4.49×10^{-01}	3.94×10^{-01}
$^{210}\text{Rn} \rightarrow ^{206}\text{Po}$	$0^+ \rightarrow 0^+$	0	6.159	0.151	$1.11 \times 10^{+03}$	$1.77 \times 10^{+03}$	$2.24 \times 10^{+03}$
$^{227}\text{Pu} \rightarrow ^{223}\text{U}$	$3/2^+_* \rightarrow 7/2^+\#$	2	8.569	0.116	6.12×10^{-03}	7.57×10^{-03}	3.82×10^{-03}
$^{223}\text{U} \rightarrow ^{219}\text{Th}$	$7/2^+\# \rightarrow 9/2^+\#$	2	9.158	0.109	3.30×10^{-05}	4.16×10^{-05}	1.24×10^{-05}
$^{219}\text{Th} \rightarrow ^{215}\text{Ra}$	$9/2^+\# \rightarrow 9/2^+\#$	0	9.506	0.130	3.84×10^{-07}	5.58×10^{-07}	2.82×10^{-07}
$^{215}\text{Ra} \rightarrow ^{211}\text{Rn}$	$9/2^+\# \rightarrow 1/2^-$	5	8.862	0.109	1.28×10^{-04}	1.41×10^{-04}	2.82×10^{-06}
$^{211}\text{Rn} \rightarrow ^{207}\text{Po}$	$1/2^- \rightarrow 5/2^-$	2	5.965	0.079	$3.53 \times 10^{+04}$	$6.44 \times 10^{+04}$	$1.85 \times 10^{+04}$

model is referred to as DDCM-M3Y. The newly discovered ^{207}Th is chosen as an example; the α -decay half lives calculated with the DDCM-RMF and DDCM-M3Y are in good agreement with the experimental data. In comparison with the DDCM-M3Y calculation, the DDCM-RMF calculations agree with experiment better.

To confirm the applicability of the present models, DDCM-RMF and DDCM-M3Y are used to calculate the α -decay half-lives for the 106 known nuclei with $89 \leq Z \leq 94$ in comparison with the empirical UDL formula. The three calculations agree with experiment well. The experimental trend of α -decay half-lives with neutron number is reproduced for the Ac, Th, Pa, U, Np, and Pu isotopes.

After verifying the reliability of the present models, especially the DDCM-RMF with more microscopic theoretical foundations, in describing α -decay, we extend the present calculations to some unknown neutron-deficient nuclei with $89 \leq Z \leq 94$. The trend of α -decay half-lives with neutron number is consistent in the three calculations. There appears a sharp decrease of α -decay half-lives between $N = 126$ and $N = 128$, which indicates that the robustness of $N = 126$ shell closure up to the Pu isotopes.

To go insight into the evolution of $N = 126$ shell closure beyond $Z = 92$, the α -preformation factor and Q_α are calculated for the neutron-deficient nuclei with $89 \leq Z \leq 94$. The preformation factors show clearly the $N = 126$ shell effect for the neutron-deficient nuclei considered here. A few irregularities in the variation of P_α in the Ac, Pa, and Np isotopes are mainly due to the presence of unpaired nuclei masking the shell effects. For the Ac–Pu isotopes with even neutron number, the behavior of Q_α as a function of neutron number is almost identical to that of P_α , which provides further strong evidence for the $N = 126$ shell effect in these neutron-deficient nuclei. These results are helpful to the experimental exploration of neutron-deficient nuclei on the extremely proton rich side.

ACKNOWLEDGMENTS

This work was partly supported by the National Natural Science Foundation of China under Grants No. 11935001 and No. 11575002; the Key Research Foundation of Education Ministry of Anhui Province under Grant No. KJ2018A0028, and the Doctoral Scientific Research Startup Fund of Anhui University (J01001319-J10113190082).

- | | |
|---|--|
| <p>[1] Z. Y. Zhang, Z. G. Gan, L. Ma, L. Yu, H. B. Yang, T. H. Huang <i>et al.</i>, <i>Phys. Rev. C</i> 89, 014308 (2014).</p> <p>[2] H. B. Yang, Z. G. Gan, Z. Y. Zhang, M. H. Huang, L. Ma, M. M. Zhang, C. X. Yuan, Y. F. Niu <i>et al.</i>, <i>Phys. Rev. C</i> 105, L051302 (2022).</p> <p>[3] K. Auranen, J. Uusitalo, H. Badran, T. Grahn, P. T. Greenlees, A. Herzan <i>et al.</i>, <i>Phys. Rev. C</i> 102, 034305 (2020).</p> <p>[4] Z. Y. Zhang, H. B. Yang, M. H. Huang, Z. G. Gan, C. X. Yuan, C. Qi <i>et al.</i>, <i>Phys. Rev. Lett.</i> 126, 152502 (2021).</p> <p>[5] H. B. Yang, Z. Y. Zhang, J. G. Wang <i>et al.</i>, <i>Eur. Phys. J. A</i> 51, 88 (2015).</p> | <p>[6] L. Ma, Z. Y. Zhang, Z. G. Gan, H. B. Yang, L. Yu, J. Jiang <i>et al.</i>, <i>Phys. Rev. C</i> 91, 051302(R) (2015).</p> <p>[7] J. Khuyagbaatar, A. Yakushev, Ch. E. Dü llmann, D. Ackermann, L.-L. Andersson, M. Block <i>et al.</i>, <i>Phys. Rev. Lett.</i> 115, 242502 (2015).</p> <p>[8] H. B. Yang, L. Ma, Z. Y. Zhang <i>et al.</i>, <i>Phys. Lett. B</i> 777, 212 (2018).</p> <p>[9] Z. Y. Zhang, Z. G. Gan, H. B. Yang, L. Ma, M. H. Huang, C. L. Yang <i>et al.</i>, <i>Phys. Rev. Lett.</i> 122, 192503 (2019).</p> <p>[10] L. Ma, Z. Y. Zhang, Z. G. Gan, X. H. Zhou, H. B. Yang, M. H. Huang <i>et al.</i>, <i>Phys. Rev. Lett.</i> 125, 032502 (2020).</p> <p>[11] M. D. Sun, Z. Liu, T. H. Huang <i>et al.</i>, <i>Phys. Lett. B</i> 771, 303 (2017).</p> |
|---|--|

- [12] T. H. Huang, W. Q. Zhang, M. D. Sun, Z. Liu, J. G. Wang, X. Y. Liu *et al.*, *Phys. Rev. C* **98**, 044302 (2018).
- [13] A. N. Andreyev, M. Huyse, P. Van Duppen, C. Qi, R. J. Liotta, S. Antalic *et al.*, *Phys. Rev. Lett.* **110**, 242502 (2013).
- [14] K. Auranen, D. Seweryniak, M. Albers, A. D. Ayangeakaa, S. Bottoni, M. P. Carpenter *et al.*, *Phys. Rev. Lett.* **121**, 182501 (2018).
- [15] G. Gamow, *Z. Phys.* **51**, 204 (1928).
- [16] R. W. Gurney and E. U. Condon, *Nature (London)* **122**, 439 (1928).
- [17] H. F. Zhang, W. Zuo, J. Q. Li, and G. Royer, *Phys. Rev. C* **74**, 017304 (2006).
- [18] K. P. Santhosh and I. Sukumaran, *Phys. Rev. C* **96**, 034619 (2017).
- [19] Z. Wang, Z. Ren, and D. Bai, *Phys. Rev. C* **101**, 054310 (2020).
- [20] M. Ismail and A. Adel, *Phys. Rev. C* **101**, 024607 (2020).
- [21] O. N. Ghodsi and M. M. Amiri, *Phys. Rev. C* **104**, 044618 (2021).
- [22] G. R. Satchler and W. G. Love, *Phys. Rep.* **55**, 183 (1979).
- [23] C. Xu and Z. Ren, *Nucl. Phys. A* **753**, 174 (2005).
- [24] C. Xu and Z. Ren, *Phys. Rev. C* **73**, 041301(R) (2006).
- [25] C. Xu and Z. Ren, *Phys. Rev. C* **74**, 014304 (2006).
- [26] B. B. Singh, M. Bhuyan, S. K. Patra, and R. K. Gupta, *J. Phys. G* **39**, 025101 (2012).
- [27] M. Bhuyan and R. Kumar, *Phys. Rev. C* **98**, 054610 (2018).
- [28] M. Bhuyan, R. Kumar, S. Rana, D. Jain, S. K. Patra, and B. V. Carlson, *Phys. Rev. C* **101**, 044603 (2020).
- [29] M. V. Chushnyakova, I. I. Gontchar, and N. A. Khmyrova, *J. Phys. G* **48**, 015101 (2021).
- [30] I. I. Gontchar, M. V. Chushnyakova, and O. M. Sukhareva, *Phys. Rev. C* **105**, 014612 (2022).
- [31] Joshua T. Majekodunmi, M. Bhuyan, D. Jain, K. Anwar, N. Abdullah, and R. Kumar, *Phys. Rev. C* **105**, 044617 (2022).
- [32] T. M. Joshua, N. Jain, R. Kumar, K. Anwar, N. Abdullah, and M. Bhuyan, *Foundations* **2**, 85 (2022).
- [33] S. Rana, R. Kumar, and M. Bhuyan, *Phys. Rev. C* **104**, 024619 (2021).
- [34] R. Kumar, S. Rana, M. Bhuyan, and P. Mohr, *Phys. Rev. C* **105**, 044606 (2022).
- [35] M. Moghaddari Amiri and O. N. Ghodsi, *Phys. Rev. C* **102**, 054602 (2020).
- [36] V. B. Soubbotin, W. von Oertzen, X. Viñas, K. A. Gridnev, and H. G. Bohlen, *Phys. Rev. C* **64**, 014601 (2001).
- [37] A. Mukherjee, D. J. Hinde, M. Dasgupta, K. Hagino, J. O. Newton, and R. D. Butt, *Phys. Rev. C* **75**, 044608 (2007).
- [38] B. Buck, A. C. Merchant, and S. M. Perez, *Phys. Rev. C* **45**, 2247 (1992).
- [39] B. Buck, A. C. Merchant, and S. M. Perez, *Phys. Rev. Lett.* **72**, 1326 (1994).
- [40] B. Buck, J. C. Johnston, A. C. Merchant, and S. M. Perez, *Phys. Rev. C* **53**, 2841 (1996).
- [41] J.-G. Deng and H.-F. Zhang, *Phys. Rev. C* **102**, 044314 (2020).
- [42] N. Wan and J. Fan, *Phys. Rev. C* **104**, 064320 (2021).
- [43] K. P. Santhosh, T. A. Jose, and N. K. Deepak, *Phys. Rev. C* **103**, 064612 (2021).
- [44] D. Deng and Z. Ren, *Phys. Rev. C* **93**, 044326 (2016).
- [45] M. Ismail and A. Adel, *Phys. Rev. C* **97**, 044301 (2018).
- [46] S. M. S. Ahmed, R. Yahaya, S. Radiman, and M. S. Yasir, *J. Phys. G* **40**, 065105 (2013).
- [47] D. Deng, Z. Ren, D. Ni, and Y. Qian, *J. Phys. G* **42**, 075106 (2015).
- [48] F. G. Kondev, M. Wang, W. J. Huang, S. Naimi, and G. Audi, *Chin. Phys. C* **45**, 030001 (2021).
- [49] W. J. Huang, M. Wang, F. G. Kondev, G. Audi, and S. Naimi, *Chin. Phys. C* **45**, 030002 (2021).
- [50] M. Wang, W. J. Huang, F. G. Kondev, G. Audi, and S. Naimi, *Chin. Phys. C* **45**, 030003 (2021).
- [51] N. Wang, M. Liu, X. Z. Wu, and J. Meng, *Phys. Lett. B* **734**, 215 (2014).
- [52] R. E. Langer, *Phys. Rev.* **51**, 669 (1937).
- [53] V. Y. Denisov and A. A. Khudenko, *Phys. Rev. C* **79**, 054614 (2009).
- [54] P. Ring, *Prog. Part. Nucl. Phys.* **37**, 193 (1996).
- [55] J. Meng, H. Toki, S. G. Zhou, S. Q. Zhang, W. H. Long, and L. S. Geng, *Prog. Part. Nucl. Phys.* **57**, 470 (2006).
- [56] J. Meng, *Relativistic Density Functional for Nuclear Structure* (World Scientific, Singapore, 2016).
- [57] B. B. Singh, S. K. Patra, and Raj K. Gupta, *Phys. Rev. C* **82**, 014607 (2010).
- [58] S. Rana, M. Bhuyan, and R. Kumar, *Phys. Rev. C* **105**, 054613 (2022).
- [59] N. Anantaraman, H. Toki, and G. F. Bertsch, *Nucl. Phys. A* **398**, 269 (1983).
- [60] K. Wildermuth and Y. Tang, *A Unified Theory of the Nucleus* (Vieweg, Braunschweig, 1977).
- [61] B. Buck, A. C. Merchant, and S. M. Perez, *At. Data Nucl. Data Tables* **54**, 53 (1993).
- [62] N. G. Kelkar and H. M. Castañeda, *Phys. Rev. C* **76**, 064605 (2007).
- [63] C. Qi, F. R. Xu, R. J. Liotta, and R. Wyss, *Phys. Rev. Lett.* **103**, 072501 (2009).
- [64] C. Qi, F. R. Xu, R. J. Liotta, R. Wyss, M. Y. Zhang, C. Asawatangtrakuldee, and D. Hu, *Phys. Rev. C* **80**, 044326 (2009).
- [65] <https://t2.lanl.gov/nis/data/astro/molnix96/spidat.html>.
- [66] C. He, Z. M. Niu, X. J. Bao, and J. Y. Guo, *Chin. Phys. C* **46**, 054102 (2022).